Paleoceanography and Paleoclimatology

RESEARCH ARTICLE
10.1029/2018PA003370

High-Resolution Benthic Mg/Ca Temperature Record of the Intermediate Water in the Denmark Strait Across D-O Stadial-Interstadial Cycles

E. G. Sessford[1], A. A. Tisserand[2], B. Risebrobakken[2], C. Andersson[2], T. Dokken[2], and E. Jansen[1,2]

[1]Department of Earth Science, Bjerknes Centre for Climate Research, University of Bergen, Bergen, Norway, [2]NORCE Norwegian Research Centre AS, Bjerknes Centre for Climate Research, Bergen, Norway

Key Points:
- Mg/Ca of benthic foraminifera indicate warm Atlantic intermediate water in the Denmark Strait during stadial and interstadial periods
- Denmark Strait stadial conditions reflect a well-stratified water column upheld in part by sea ice and brine rejection
- Multiproxy records indicate that interstadial oceanographic conditions in the Denmark Strait were unstable and rapidly varying

Correspondence to:
E. G. Sessford,
evangeline.sessford@uib.no

Citation:
Sessford, E. G., Tisserand, A. A., Risebrobakken, B., Andersson, C., Dokken, T., & Jansen, E. (2018). High-resolution benthic Mg/Ca temperature record of the intermediate water in the Denmark Strait across D-O stadial-interstadial cycles. *Paleoceanography and Paleoclimatology*, *33*, 1169–1185. https://doi.org/10.1029/2018PA003370

Received 21 MAR 2018
Accepted 17 OCT 2018
Accepted article online 19 OCT 2018
Published online 5 NOV 2018

The copyright line for this article was changed on 29 NOV 2018 after original online publication.

Abstract Dansgaard-Oeschger (D-O) climate instabilities that took place during Marine Isotope Stage 3 are connected to changes in ocean circulation patterns and sea ice cover. Here we explore in detail the configuration of the water column of the Denmark Strait during D-O events 8–5. How the ocean currents and water masses within the Denmark Strait region responded and were connected to the North Atlantic are discussed. We investigate sediment core GS15-198-36CC, from the northern side of the Greenland-Iceland Ridge, at 30-year temporal resolution. Stable carbon and oxygen isotope reconstructions based on benthic foraminifera, together with a high-resolution benthic foraminiferal record of Mg/Ca paleothermometry, is presented. The site was bathed by warm intermediate waters during stadials and cool but gradually warming intermediate water during interstadials. We suggest that stadial conditions in the Denmark Strait are characterized by a well-stratified water column with a warm intermediate water mass that lies beneath a cold fresh body of water where sea ice and brine rejection work in consort to uphold the halocline conditions. Interstadial periods are not a pure replicate of modern times, but rather have two modes of operation, one similar to today, and the other incorporating a brief period of warm intermediate water and increased ventilation.

Plain Language Summary During the last ice age (30–40 thousand years ago), rapid warmings—Dansgaard-Oeschger events—up to 15 °C occurred over Greenland resulting in Arctic air temperature warmings, droughts over Africa, stronger monsoons over Asia, and global sea level. These climatic changes are connected by the global telecommunicator: the Atlantic Meridional Overturning Circulation, which is largely driven by changes in ocean water properties that take place in the Denmark Strait. We use sediment cores from the Denmark Strait to extract archives of past abrupt change in ocean temperature to investigate the dynamic changes in ocean circulation across Dansgaard-Oeschger events. Geochemical analysis of microfossils that lived on the seafloor reveals that during the cold periods the presence of sea ice is linked to warming waters at intermediate depth in the Denmark Strait and likely a decrease in the strength of the overturning circulation. During the warm period, intermediate waters cooled suggesting a heat release to the atmosphere due to the absence of sea ice. Our research indicates that the absence or presence of Arctic sea ice is linked to these climate disturbances in the past and is likely linked to the global climate changes the Earth is experiencing today.

1. Introduction

The Arctic and Nordic Seas regions are currently undergoing major and fast changes in sea ice cover and ocean properties. Abrupt changes in ocean circulation and sea ice cover in the past may shed light on processes involved in such changes, which may be relevant for the present situation, even if they occurred under different climatic boundary states. The last glacial cycle is highlighted by a series of abrupt climatic excursions commonly referred to as Dansgaard-Oeschger (D-O) events (Dansgaard et al., 1993). These events correspond to high amplitude changes in oxygen isotopes ($\delta^{18}O$) as recorded in multiple Greenland ice cores and relate to rapid transitions from cold Greenland Stadial (GS) into warm Greenland Interstadials (GI) and stepwise gradual retreat back into stadial conditions (Dansgaard et al., 1993; Rasmussen et al., 2014; Voelker, 2002). The atmospheric temperature changes recorded in the Greenland ice cores are also identified in marine sediment cores as hydrographic changes in the Nordic Seas (Dokken et al., 2013; Kissel et al., 1999;

Rahmstorf, 2002; van Kreveld et al., 2000; Voelker, 2002; Voelker et al., 2000; Voelker & Haflidason, 2015). Multiproxy records from sediment cores across the Nordic Seas are commonly used to describe and detect changes in the vertical distribution of the water masses at different locations and across GS and GI periods and transitions. However, one key area is missing: proxy records documenting changes in intermediate water in the Denmark Strait.

Within the shallow regions of the Denmark strait three significant water masses pass over the sill: warm Atlantic Surface water, cold Polar Surface Water (PSW), and cold Denmark Strait Overflow Water (Rudels et al., 2005). The strength, temperature, and convection rate of these water masses directly impact the rate of Atlantic Meridional Overturning Circulation (AMOC) (Logemann & Harms, 2006). During the D-O events changes in water properties were common from Stadial to Interstadial period (van Kreveld et al., 2000; Voelker, 2002; Voelker et al., 2000). Some studies reconstructing upper water column conditions during D-O events exist for the Denmark Strait region. Voelker et al. (2000) reconstructed the upper water column during D-O events by utilizing $\delta^{18}O$ and $\delta^{13}C$ of *Neoglobiquadrina pachyderma* (*N. pachyderma*/NP) and iceberg rafted detritus (IRD) as surface proxies. They suggest that less ventilated and less saline surface water (lower $\delta^{13}C_{NP}$ and $\delta^{18}O_{NP}$ values) are associated with iceberg discharge and melting during GS as indicated by high IRD values. Greenland interstadials were generally associated with more saline surface water (higher $\delta^{18}O_{NP}$ values) and better ventilation. Results from the Irminger Sea, south of the Greenland-Iceland Ridge by van Kreveld et al. (2000), also reflect saltier surface waters during GI, and transfer functions on planktonic foraminifera assemblage counts indicate warm subsurface sea temperatures (up to 8 °C). Assessments of bottom water changes using epibenthic foraminifera $\delta^{18}O$ and $\delta^{13}C$ minima from south of the sill in the Irminger Sea have been used to argue for short-lasting spikes in brine water production due to sea ice formation in salt-depleted meltwater influenced surface waters, specifically toward the end of a GS (van Kreveld et al., 2000).

The vertical distribution of water masses and their properties have been extensively examined in the Norwegian Sea for D-O events 8–5. The majority of these studies show a vertical distribution of water masses during GI that reflect conditions comparable to today with an active, warm Atlantic Water (AW) inflow to the Nordic Seas at the surface, underlain by cold, deep waters overflowing back to the North Atlantic that were generated by open ocean convection within the Nordic Seas (Dokken et al., 2013; Dokken & Jansen, 1999; Ezat et al., 2014, 2017; Rasmussen & Thomsen, 2004). These studies suggest that during GS, a thickening and deepening of the warm Atlantic inflow down to at least 1,179 m (Ezat et al., 2014) as an intermediate layer beneath a cold fresh surface layer developed a halocline and led to greatly reduced convection and therefore a decline in cold overflow water during GS (Dokken et al., 2013; Dokken & Jansen, 1999; Ezat et al., 2014; Rasmussen & Thomsen, 2004). Over half of the modern cold overflow water from the Nordic Seas, 4.3 of 7.9 Sv, flows southward through the Denmark Strait (Nilsen et al., 2003). Despite the importance of the Denmark Strait area, there are no published studies investigating changes in the Denmark Strait intermediate water during D-O events or how these changes are related to the overall changes in the Nordic Seas oceanography.

Conceptual theories concerning the mechanisms influencing the hydrography and development of the halocline vary. Rasmussen and Thomsen (2004) propose increases in fresh water due to glacier runoff, whereas Dokken et al. (2013) argue for an additional role of increased sea ice cover and brine rejection. Contrasting aforementioned theories, Eynaud et al. (2002) and Wary et al. (2017) argue, based on dinocyst assemblage results from the Norwegian Sea, that the cold homogenous surface waters and the presence of annual sea ice cover are rather properties associated with GI and that there continues to be an active deep convection during GI due to brine release. A strong reduction in convection during GS is therefore argued to be a result of the occurrence of a strong halocline and seasonal thermocline dividing the cold fresher surface layers with the warm saline layers below (Eynaud et al., 2002; Wary et al., 2015, 2017).

We provide the first benthic temperature reconstruction from the western Nordic Seas to clarify the situation in the Denmark Strait during D-O events and contribute to testing the validity of the various conceptual theories for the role of the Nordic Seas through (1) increasing the sediment core proxy records for the D-O events 8–5 to include intermediate water from the Denmark Strait; (2) implementing Mg/Ca measurements and calibrations on benthic foraminifera to reconstruct intermediate water temperatures, and benthic $\delta^{13}C$ and $\delta^{18}O$ stable isotopes to elucidate the exchange of warm inflow versus cold outflow over the Greenland-Iceland Ridge during D-O events 8–5; (3) constraining changes in the oxygen isotopic composition of the ambient

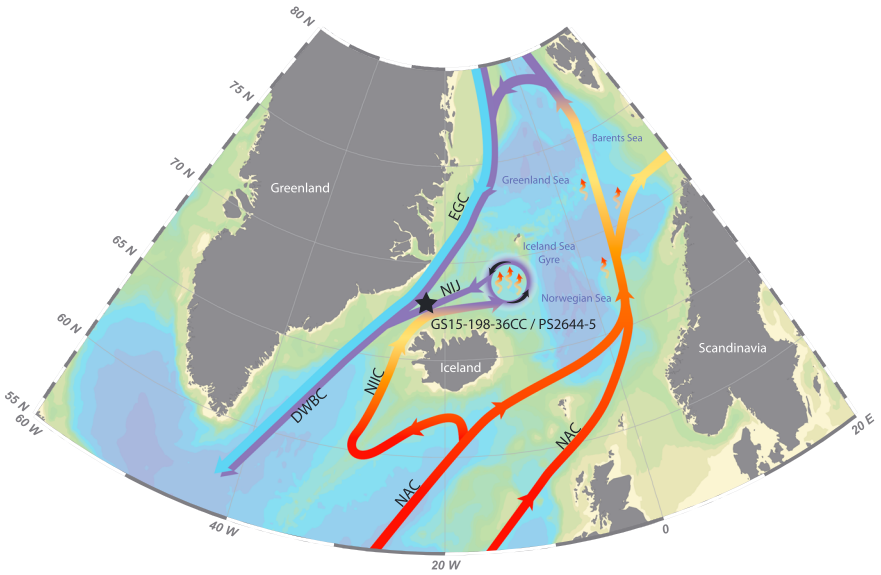

Figure 1. Modern overturning circulation in the Iceland Sea (adapted from Våge et al., 2013) and location of the cores GS15-198-36CC, which is the primary core used in this study (770-m water depth), alongside some supporting material from core PS2644-5, marked with a star. Acronyms are: North Atlantic Current (NAC), Northern Icelandic Irminger Current (NIIC), The Northern Icelandic Jet (NIJ), East Greenland Current (EGC), and Deep Western Boundary Current (DWBC). Map image originates from Ocean Data View (ODV) (Schlitzer, 2014).

ocean waters (δ_w) and thus determining the role of subsurface warming versus changing δ_w on calcite $\delta^{18}O$; and (4) confirming the role of brines in the regional oceanography through construction of the oxygen composition of ambient ocean water (δ_w) record (from combined Mg/Ca and $\delta^{18}O$ analysis). With increased knowledge of the vertical water column changes within the Denmark Strait we can then begin to deduce and discuss changes in deepwater formation and changes in circulation and convection in the Nordic Seas between GI and GS periods.

2. Oceanographic Setting and Study Site

Under the present interglacial conditions, the Denmark Strait exhibits a complex system of water mass exchange between the Nordic Seas and the North Atlantic (Figure 1). Northward surface flow of the Northern Icelandic Irminger Current (NIIC) brings warm (1.5 to 10 °C) and saline (34.92 to 35.2 psu) AW from the North Atlantic over the Icelandic Shelf and vicinity of the shelf break to the Iceland Sea Gyre (Jonsson & Valdimarsson, 2004; Swift & Aagaard, 1981; Våge et al., 2011, 2013). In the Iceland Sea Gyre, the AW loses its heat to the atmosphere and is transformed into dense water making up the majority of the Denmark Strait Overflow Waters (DSOW). The DSOW return to the North Atlantic as an intermediate water mass via the Northern Icelandic Jet (NIJ) (Jonsson & Valdimarsson, 2004, 2012; Våge et al., 2011). The origins of the DSOW are highly debated within the modern community (Eldevik et al., 2009; Jeansson et al., 2008); however, to remain consistent within this text we rely on the Våge et al. (2011, 2013) circulation scheme for discussions. Våge et al. (2013) refer to this particular contribution to the DSOW as Atlantic Origin Overflow Water (Atl; $>$ 0 °C), and it appears to consistently lie around the 650-m isobath. The Atl comprises the bulk of the NIJ and is distinguished from deeper Arctic Origin Overflow Water (Arc; $<$ 0 °C), another contributor to the DSOW, by its higher temperatures and convection location (Våge et al., 2013). The Atlantic Ocean is ultimately the original source for both Atl and Arc, and their labels mainly indicate the geographical domain in which they transform from surface to intermediate water (Våge et al., 2011). The Atl formation takes place along the Norwegian continental slope when surface AW flowing northward within the NAC densifies, whereas wintertime convection within the interior Greenland and Iceland seas produces Arc (Våge et al., 2011). Arc water is banked up high on the Iceland continental slope and forms the densest component of the DSOW supplied by the NIJ. Another contributor to the DSOW is the East Greenland Current (EGC).

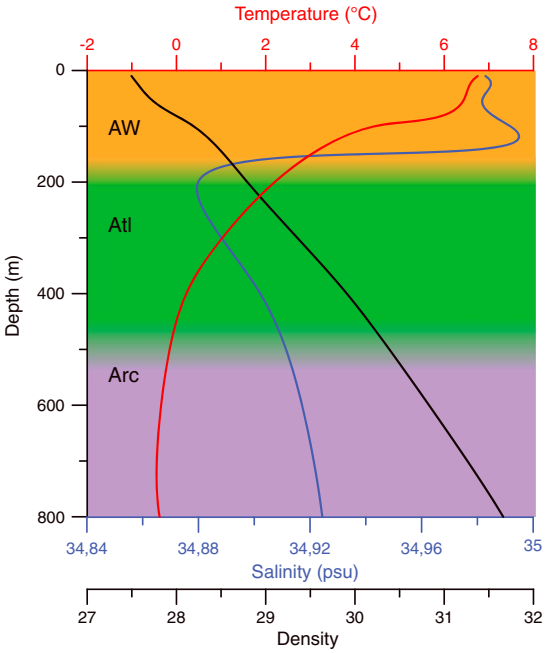

Figure 2. Conductivity, temperature, and depth (CTD) profile for site GS15-198-36CC measured on 26 July 2015. Water masses are indicated based on descriptions by Våge et al. (2013) and as used in the text, Atlantic Water (AW), Atlantic Origin Overflow Water (Atl) and Arctic Origin Overflow Water (Arc). Density calculations derived using Web resources found at http://www.csgnetwork.com/water_density_calculator.html and based off work from Millero et al. (1980). Note that the absence of Polar Surface Water (PSW) is not a consistent trait of this location.

The surface water of the EGC is made up of cold (−2 to 0 °C) and relatively fresh (<31 to 34.85 psu) PSW, carrying ice and extending across most of the DS (Jeansson et al., 2008; Våge et al., 2013). Most of the liquid freshwater flows southward and does not flow into the convective regions north of Iceland; icebergs originating from Greenland, solid sea ice and sea ice brine are, however, liable to also end up in the Iceland Sea Gyre (Dodd et al., 2012). The intermediate and deep waters of the EGC are fed by modified AW recirculating from the Fram Strait and waters formed in the Greenland and Iceland Seas (Jeansson et al., 2008; Rudels, 2002). Våge et al. (2011, 2013) find that these waters are not only confined to the Greenland shelf and slope but are also associated with a separated EGC in the interior of the Denmark Strait. This separated EGC is thought to vary in both strength and laterally across the Denmark Strait over time (Våge et al., 2011, 2013). Variations in the position and strength of the EGC and NIJ are highly variable on all time scales and are thought to largely depend on sea ice production and transport from the Arctic to the North Atlantic (Köhl et al., 2007; Mauritzen & Häkkinen, 1997). In turn, the presence or lack of sea ice is largely dependent on the positioning and strength of the warm inflowing NIIC (Logemann & Harms, 2006; Solignac et al., 2006). The Deep Western Boundary Current (DWBC), which is fed by the DSOW, is therefore susceptible to any changes in temperature or positioning of the NIIC (Dickson et al., 2008; Jeansson et al., 2008).

Our core was obtained from the northern side of the Greenland-Iceland Ridge within the Denmark Strait at 770-m water depth (Figure 1). The core site lies almost directly on the northern part of the Hornbanki hydrographic section as described by Jonsson and Valdimarsson (2004), west of the Kolbeinsey Ridge (Jonsson & Valdimarsson, 2012) and very close to the present boundary between the NIJ and the separated EGC (Våge et al., 2013). At the time of core collection, warm and saline surface water flowed in the NIIC over the core site to a depth of approximately 150 m where the halocline lay (Figure 2). Potential temperatures and salinity at our coring site have been measured by conductivity, temperature depth sensors (CTD), 26 July 2015 recording −0.38, 0.22, and 4.44 °C and 34.92, 34.90, and 34.99 psu at 770, 400, and 100 m, respectively (Figure 2). These depths align with AW, Atl, and Arc, respectively (Figure 2). Oxygen isotopic analyses of bottom water obtained from 760-m water depth at the time of coring gave a $\delta^{18}O_{SW}$ of 0.41‰. Extracted GLODAPv2 data (Olsen et al., 2016) from 66 to 69°N and 19–30°W produced average carbonate ion saturation ($\Delta[CO]_3^{2-}$) values of seawater to be 52.07 μmol/kg (>500 m), 62.22 μmol/kg (500 m > <150 m), and 73.94 μmol/kg (>150 m). The $\Delta[CO]_3^{2-}$ were calculated from tCO^2 and alkalinity at in situ temperature, pressure, phosphate, and silicate and implemented the dissociation constants from Lueker et al. (2000). For this reason, the modern waters are not considered to be undersaturated in respect to calcite.

3. Materials and Methods

The Calypso core GS15-198-36CC (67°51′N, 21°52′W, water depth 770 m) was retrieved during an Ice2Ice cruise onboard R/V *G.O. Sars* in July 2015 (Figure 1). Magnetic susceptibility measurements were conducted onboard at the time of core retrieval, using a hand-held Bartington MS3 Magnetic Susceptibility meter with a MS2E surface Scanning Sensor. Measurements were carried out at 1-cm intervals.

Samples were obtained at 0.5-cm intervals, and each sample was wet sieved over 63-, 150-, and 500-μm sieves, oven dried, and the >150 μm fraction was further dry sieved to narrow sample size to between 150 and 212 μm for the geochemical analyses. Every 5 cm the absolute abundance of the benthic foraminifera, *Elphidium excavatum*, was counted, and planktic foraminifera, *N. pachyderma*, were picked to run for isotopes. Specimens of the benthic foraminifera, *Cassidulina neoteretis*, were hand-picked every 0.5 cm. All *C. neoteretis* specimens were counted for determination of absolute

abundance and subsequent selection of only the most pristine individuals for geochemical analysis. The majority of samples (127 of 184) contained enough specimens to retain the 0.5 cm sample spacing; however, in some cases where the abundance was too low to run all geochemical analyses, two to four samples were combined together (35, 14, and 8 samples in 1-, 1.5-, and 2-cm resolution, respectively). Shells of *C. neoteretis* were gently crushed between two glass plates under a microscope to allow visual contaminants to be removed, homogenized, and then split into at least two aliquots; one approximately 40–80 μg to be cleaned and analyzed for stable isotopes and the other 300–360 μg for measuring Mg/Ca. In some cases where there was enough sample a third aliquot has been saved to run for replicates or further analysis.

Aliquots for isotope analysis were cleaned using methanol and ultrasonicated for 5 s, dried, and then run on a Kiel IV preparation line coupled to a Thermo Finnigan MAT 253 at FARLAB at the University of Bergen. Results are reported relative to Vienna Pee Dee Belemnite (VPDB), calibrated using NBS-19 and crosschecked with NBS-18. Long-term reproducibility (1 s) of in-house standards for samples between 10 and 100 μg is ≤0.08‰ and 0.03‰ for $\delta^{18}O$ and $\delta^{13}C$, respectively.

The samples for trace element analysis were cleaned following the procedure described by Boyle and Keigwin (1985) and Barker et al. (2003) and included clay removal, reductive, oxidative, and weak acid leaching steps. All samples were dissolved in trace metal pure 0.1 M HNO_3 and diluted to a final concentration of 40 ppm of calcium. Trace elements were measured at the Trace Element Lab (TELab) at Uni Research Climate, Bergen (Norway) on an Agilent 720 inductively coupled plasma optical emission spectrometer (ICP-OES) against standards with matched calcium concentration to reduce matrix effects (Rosenthal et al., 1999). Six standards have been prepared at TELab and have a composition similar to foraminiferal carbonate (0.5–7.66 mmol/mol). Every eight samples, known standard solution with Mg/Ca ratio of 5.076 mmol/mol was analyzed to correct for instrumental biases and analytical drift of the instrument. Long-term Mg/Ca analytical precision, based on standard solution is ±0.026 mmol/mol (1σ standard deviation) or 0.48% (relative standard deviation). Average reproducibility of duplicate measurements (pooled standard deviation, dof = 18) is equivalent to an overall average precision of 3.25%. The average Mg/Ca of long-term international limestone standard (ECRM752-1) measurements is 3.76 mmol/mol (1σ = 0.07 mmol/mol) with the average published value of 3.75 mmol/mol (Greaves et al., 2008).

The r^2 of regression between Mg/Ca and Fe/Ca, Al/Ca, and Mn/Ca are 0.027, 0.001, and 0.013, respectively, indicating no systematic contamination due to insufficient cleaning. The average downcore measurements for Fe/Ca, Al/Ca, and Mn/Ca analyses in *C. neoteretis* are 42, 299, and 267 μmol/mol, respectively. Fe/Ca and Al/Ca are well below contamination limits, 100 μmol/mol (Fe/Ca) and 400 μmol/mol (Al/Ca) (Barker et al., 2003; Barrientos et al., 2018; Skinner et al., 2003; Skirbekk et al., 2016). The measured Mn/Ca ratios are over the 105 μmol/mol limit as determined by Boyle (1983) and covary in some sections of the downcore measurements (Figure 3), which indicates that our samples have the potential to be contaminated by ferromanganese precipitate. However, being an infaunal species *C. neoteretis* can be expected to have high Mn/Ca ratios indicating a strong influence of hypoxic conditions rather than temperature on the incorporation of Mn into the foraminifera shell (Groeneveld & Filipsson, 2013; Hasenfratz et al., 2017; Skinner et al., 2003). Therefore, although the possibility of contamination cannot be ruled out, temperature is assumed to be the dominant control on the Mg/Ca variability in *C. neoteretis* in this study.

There are two published Mg/Ca calibrations for *C. neoteretis*. (Mg/Ca = 0.864(±0.07) * exp(0.082(±0.02) * BWT)) is based on core top data from Kristjánsdóttir et al. (2007), covering a water depth from 211 to 483 m with a Mg/Ca range of 0.93–1.38 mmol/mol and a temperature range of 0.96–5.47 °C. Mg/Ca = 1.009(±0.02) * exp(0.042(±0.01) * BWT)) from Barrientos et al. (2018) incorporates core tops from Kristjánsdóttir et al. (2007) and 15 new core top measurements (Table 1 and Figure 4). The Barrientos et al. (2018) calibration covers a water depth from 159 to 1118 m with a Mg/Ca range of 0.84–1.38 mmol/mol and a temperature range of −0.10 to 5.47 °C. Only 25% and 47% of our measured samples, respectively, fit within the Kristjánsdóttir et al. (2007) and Barrientos et al. (2018) Mg/Ca ratio range of these calibrations. Both of these calibrations give unrealistically cold end temperatures down to −3.4 and −10 °C (Kristjánsdóttir et al., 2007; Barrientos et al., 2018, respectively) when applying this calibration to our Mg/Ca data set. The Barrientos et al. (2018) Mg/Ca range has a wide spread over a very narrow

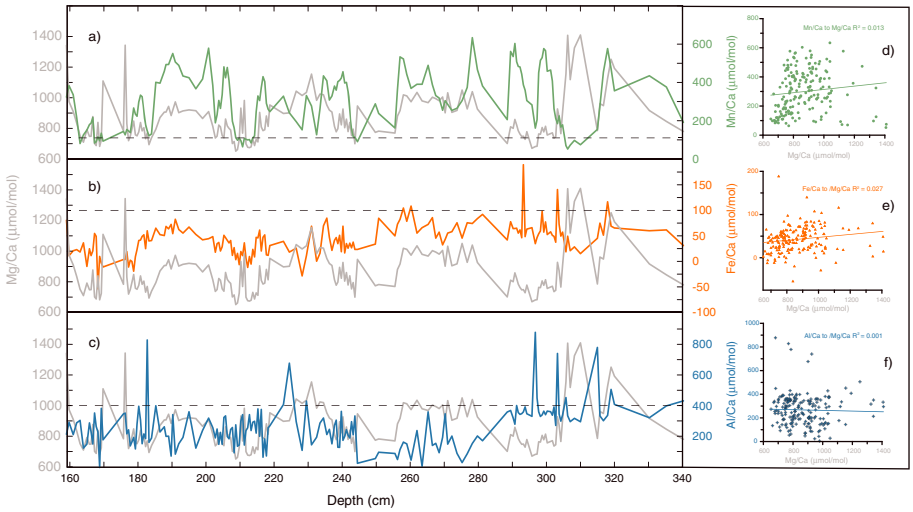

Figure 3. Trace element content of *C. neoteretis* samples analyzed for Mg/Ca. Downcore contaminants (a-c) of Mn/Ca (green), Fe/Ca (red) and Al/Ca (blue) to Mg/Ca (grey) indicating general contamination limits with black dashed lines for each element. C-d) Scatter of Mn/Ca (green), Fe/Ca (red) and Al/Ca (blue) plotted against Mg/Ca showing no covariance between these trace metals.

temperature interval, and the resulting temperatures for our Mg/Ca ratios become excessively cold, well below physically realistic values. The Kristjánsdóttir et al. (2007) calibration gives the least unrealistic values, and the core tops are from the same region as we investigate. Therefore, we opted to use the calibration from Kristjánsdóttir et al. (2007) but modified it slightly to address the too cold temperature end-member issue in two ways: first by adding a modern, Rose Bengal stained core top sample from our study site (GS15-198-36MCA; Table 1) and second by attempting two alternative *C. neoteretis* calibration equations that force the cold end-member data to realistic values by adding a cold end cutoff temperature of −0.38 and −1.8 °C for our four lowest Mg/Ca measurements (Table 1). The temperature −1.8 °C was chosen as the absolute coldest temperature physically obtainable within the

Table 1
Sample Data Used in Mg/Ca-Temperature Calibration Equation

Number	Core site	Depth (m)	ICT[a] (°C)	Mg/Ca (mmol/mol)	Reference
1	B997-314	245	5.07	1.241	Kristjánsdóttir et al. (2007)
2	B997-315	211	5.07	1.377	Kristjánsdóttir et al. (2007)
3	B997-321	483	1.43	1.0	Kristjánsdóttir et al. (2007)
4	B997-324	278	3.87	1.286	Kristjánsdóttir et al. (2007)
5	B997-326	362	2.07	0.987	Kristjánsdóttir et al. (2007)
6	B997-327	360	4.51	1.158	Kristjánsdóttir et al. (2007)
7	B997-337	220	5.47	1.355	Kristjánsdóttir et al. (2007)
8	B997-337	220	5.47	1.379	Kristjánsdóttir et al. (2007)
9	BS11-91-K15	445	0.96	0.927	Kristjánsdóttir et al. (2007)
10	BS11-91-K15	445	0.96	0.933	Kristjánsdóttir et al. (2007)
11	GS15-198-36CC	770	−0.38 (−1.8)	0.652	This Study
12	GS15-198-36CC	770	−0.38 (−1.8)	0.662	This Study
13	GS15-198-36CC	770	−0.38 (−1.8)	0.670	This Study
14	GS15-198-36CC	770	−0.38 (−1.8)	0.674	This Study
15	GS15-198-36MCA	770	−0.38	0.847	This Study

[a]Isotopic calcification temperature from modern sites (excluding core site BS11-91-K15, which does not have bottom water $\delta^{18}O_{seawater}$ measurements and have therefore used the CTD temperature for this site (see (Kristjánsdóttir et al., 2007, p. 16) for details), and site GS15-198-36 that assumes the coldest measured Mg/Ca ratios from down core samples to have a cutoff of −1.8 °C (the coldest possible Arctic water temperature) or −0.38 °C, the measured BWT at site GS15–198-36 in modern times. Note that numbers 11–14 are appointed Mg/Ca values and not measured, whereas number 15 is a Rose Bengal stained core top sample

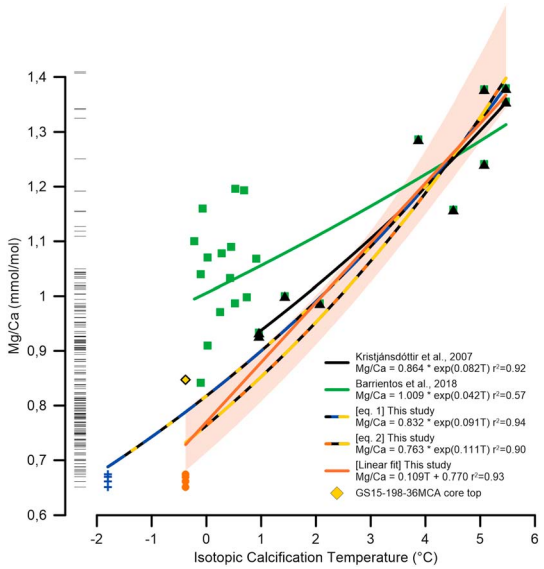

Figure 4. Mg/Ca versus isotopic calcification temperature, exponential calibrations for the benthic species *C. neoteretis* that are discussed in this study. Temperatures referred to in the text use equation (2) plotted here in orange/yellow/black line with sample points shown with orange circles (arbitrary temperature from Table 1), yellow diamond (Core top, Table 1) and black triangles (Kristjánsdóttir et al. (2007) Table 1), and a 95% confidence envelope. The original data points as used in Kristjánsdóttir et al. (2007) are in black triangles and black line; the calibration with a low end-member of −1.8 °C (equation (1)) are shown in navy/yellow/black line and incorporates the navy plus symbols (arbitrary temperature from Table 1), yellow diamond (Core top, Table 1) and black triangles (Kristjánsdóttir et al., 2007; Table 1). See Kristjánsdóttir et al. (2007) and Table 1 for details concerning the calibration and isotopic calcification of temperatures. The green line and green squares are from the Barrientos et al. (2018) calibration that is not used in this study. The solid orange line is the linear calculation formed from the same sample points as equation (2) and is not discussed further in the text. The black bar on the left of the figure indicates the Mg/Ca measurement range of all 180 measurements for this study. Note how the majority of measurements are outside of the Kristjánsdóttir et al. (2007) temperature calibration range.

Arctic Ocean Waters during modern times (Rudels et al., 2000) and −0.38 °C chosen as the modern potential temperature measured on this site (Figure 2). This results in two exponential curves expressed as

$$Mg/Ca = 0.832(\pm 0.03)^{*}\ \exp(0.091(\pm 0.02)*BWT) \qquad R^2 = 0.94, \quad (1)$$

$$Mg/Ca = 0.763(\pm 0.05)^{*}\ \exp(0.111(\pm 0.02)*BWT) \qquad R^2 = 0.90 \quad (2)$$

for an end-member cutoff of −1.8 and −0.38 °C, respectively (Figure 4). A 2σ temperature error (95% confidence level) for equation (2) results in temperature uncertainty of ±0.64 to ±0.97 °C for the temperature range (−1.45–5.66 °C) covered by the core GS15-198-36CC. Further discussions and use of Mg/Ca derived temperatures within this article will use the calibration as expressed for the end member cutoff of −0.38 °C (equation (2)) as we believe this to be a conservative estimate of how warm the bottom water at our site would be during glacial times. For the region, it is within the middle range for modern bottom water temperature as shown in Våge et al. (2013).

When calculating the stable oxygen composition of ocean water (δ_w), the $\delta^{18}O$ sea level corrections follow the sea level reconstruction from Waelbroeck et al. (2002). One meter of sea level change is considered to represent a 0.009‰ change in $\delta^{18}O$ (Adkins et al., 2002; Elderfield et al., 2012; Schrag et al., 1996; Shackleton, 1974). The mean *C. neoteretis* $\delta^{18}O$ of the Late Holocene (0–3.6 ka BP) value from MD95-2011 (4.1‰), representing intermediate water depths in the eastern Nordic Seas (Risebrobakken et al., 2003), is used as a modern reference for the down-core sea level corrections. We calculated temperature using (equation (2)) and use the temperature from the CTD potential temperature at 770-m depth, −0.38 °C. Oxygen isotope-based temperature estimates are generated using the 0.25‰/1 °C relationship, which is close to linear for this temperature range (Marchitto et al., 2014). The difference between VPDB and δ_w is corrected for using a constant of 0.3‰. Hence, the relative change in δ_w at site GS15-198-36 can be explained by: δ_w = (sea level (m) * 0.0092) − (($T_{top} - T_{Down}$) * 0.23) + 0.3 where T_{top} is the temperature at core top (or CTD) in °C and T_{down} is the down core temperature in °C as measured on the foraminifera samples.

4. Chronology

Cores GS15-198-36CC and PS2644-5 (67°52.02′N, 21°45.92′W, 777-m water depth Voelker and Haflidason (2015)) are for all essential purposes, from the same location. When establishing the age model of GS15-198-36CC, we rely on the published age model established for PS2644-5. The previously published age model of PS2644-5 is based on 80 ^{14}C dates, and the assumption that meltwater events recorded in the PS2644-5 core coincided with GS and cooling episodes with periods of large iceberg release from ice sheets (Voelker et al., 1998, 2000; Voelker & Haflidason, 2015). The first step we did to establish the age model of GS15-198-36CC was to tune the magnetic susceptibility record of GS15-198-36CC to the magnetic susceptibility record from PS2644-5 (Laj, 2003), to establish the correct D-O events and approximate ages. Next, we rely on a stratigraphic tuning of the marine records to the NGRIP $\delta^{18}O$ record to further refine the chronology (Figure 5). The PS2644-5 core is previously tuned to the $\delta^{18}O$ from NGRIP using $\delta^{18}O$ of *N. pachyderma* (Voelker & Haflidason, 2015). To avoid dependence on interpretations of water mass changes, we instead tune the high-frequency variations in magnetic susceptibility in the marine core to the NGRIP $\delta^{18}O$ record on the GICC05 timescale (Svensson et al., 2008), using AnalySeries 2.0 (Paillard et al., 1996). This results in

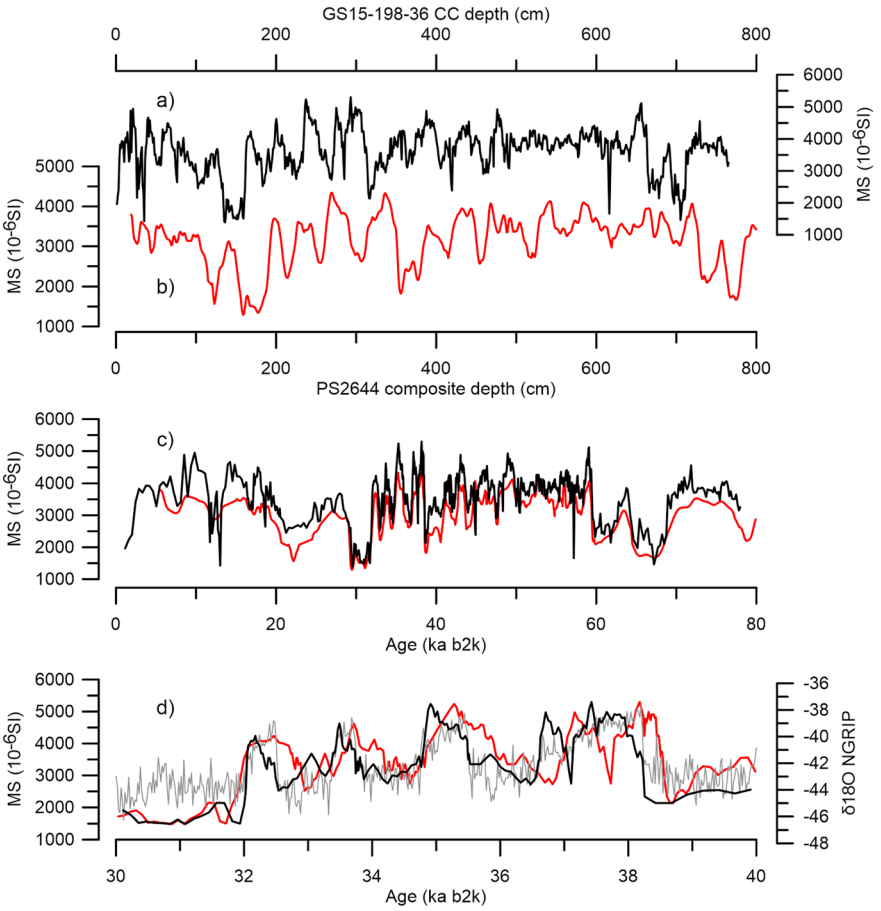

Figure 5. Age model development of core GS15-198-36CC based on magnetic susceptibility (MS) using core PS2644-5 as an age indicator where (a) shows MS of GS15-198-36CC versus original depth, (b) shows MS of PS2644-5 versus original depth, (c) shows MS for both cores on the PS2644-5 age model revealing how very similar the cores are, and (d) shows MS of GS15-198-36CC using the PS2644-5 age model in relation to the NGRIP $\delta^{18}O$ transitions in red (note the offset), and the MS for GS15-198-36CC using the new age model of this study in relation to the NGRIP $\delta^{18}O$ transitions on the GICC05 timescale (black). The red lines are the PS core, the black are for GS15-198-36CC, and the grey are for NGRIP.

an offset of approximately 150 years from the PS2644-5 age model. It has been shown that the rapid oscillations in magnetic properties during MIS3 in the North Atlantic/Nordic Seas are coherent with changes in the $\delta^{18}O$ record of Greenland (Kissel et al., 1999). Throughout the paper, all data from GS15-198-36CC and PS2644-5 are shown on the same age scale, tuned to NGRIP based on magnetic susceptibility.

5. Proxy Description and Use

Cassidulina neoteretis is a shallow infaunal benthic foraminifera species (Jansen et al., 1990) and known to live in cooled and modified AW with optimal temperatures, and therefore highest abundance, around −1 °C (Jennings & Helgadottir, 1994; Mackensen & Hald, 1988; Seidenkrantz, 1995) but are known to survive in waters up to 5 °C (Kristjánsdóttir et al., 2007). They are often associated with fine-grained, organic-rich terrigenous mud, that is, plenty of food particle sedimentation, and weak bottom currents (Lorenz, 2005; Mackensen & Hald, 1988; Seidenkrantz, 1995). However, they may also relate to high nutrient contents found in the occurrence of phytoplankton blooms, which can also be present beneath sea ice (Arrigo et al., 2012; Jennings et al., 2004; Lubinski et al., 2001). *Cassidulina neoteretis* tends to prosper in stable marine environments with salinity of 34.91–34.92 psu and is often associated with glacial episodes or periods (Mackensen & Hald, 1988). *Elphidium excavatum* is known to dominate in highly unstable and turbid environments and is most commonly found living in shallow water (Rytter et al., 2002). It is therefore often assumed that if found off the shallow shelves, it has

been reworked posthumous during periods with stronger currents (Hald et al., 1994). Changes in absolute abundance of *C. neoteretis* and *E. excavatum* are used to argue for changes in type of water mass bathing GS15-198-36CC during D-O events 8–5. For example, periods with the highest abundance (greater than 20 #/g dry bulk sediment) of *C. neoteretis* are linked to Arc water, periods with middle range abundance (greater than 5 and less than 20 #/g dry bulk sediment) are linked to Atl water, and periods with the lowest (less than 5 #/g dry bulk sediment) or no specimens at all are linked to AW. The increased presence of *E. excavatum* is linked to stronger currents or a shift in current boundary, that is, more unstable environment.

The stable high percentage of *N. pachyderma* from core PS2644-5 is used as an argument to support the continued presence of cold polar water at the surface or near surface throughout the stadial-interstadial period. *Neoglobiquadrina pachyderma* moves vertically throughout the top of the water column to depths down to 300 m to try and avoid low salinity environments (Carstens et al., 1997) and aids to justify surface depth interpretations in our discussions.

Oxygen isotopes of foraminiferal calcite are commonly used to reconstruct changes between stadial-interstadial cycles (Dokken et al., 2013; Ezat et al., 2014; Ravelo & Hillaire-Marcel, 2007). $\delta^{18}O$ in foraminifera are a function of seawater $\delta^{18}O$, which is linked to glacio-eustatic changes and salinity, and of temperature (Ezat et al., 2014; Marchitto et al., 2014). In addition, brine rejection through sea ice formation will provide water masses with low $\delta^{18}O$ and relatively high salinity (Craig & Gordon, 1965). We use planktic $\delta^{18}O_{NP}$ of PS2644-5 as an indicator of the influence of near surface freshwater as demonstrated by Voelker and Haflidason (2015) where light $\delta^{18}O_{NP}$ is an indicator of fresher surface water, and heavy $\delta^{18}O_{NP}$ of more saline surface water. Benthic $\delta^{18}O_{CN}$, which is remarkably similar to NGRIP $\delta^{18}O$ in their shape and amplitude, is used, following Dokken et al. (2013), to infer presence of sea ice formation and concurrent brine rejection when $\delta^{18}O_{CN}$ is light and open ocean when $\delta^{18}O_{CN}$ is heavy.

The isotopic signature of carbon in foraminiferal calcite is related to ventilation and water mass age (Dokken et al., 2013; Ravelo & Hillaire-Marcel, 2007). When the sea surface is covered by sea ice, surface exchange of CO_2 is inhibited; the seawater ^{13}C decreases due to aging and supply of ^{12}C from gradual decomposition of organic matter. We therefore infer that lower $\delta^{13}C_{CN}$ values are an indicator of extensive sea ice cover and less ventilation and higher values reflect sea ice free and well-ventilated conditions.

Mg/Ca measurements of *C. neoteretis* are applied to the Mg/Ca temperature calibration (equation (2)) to reconstruct past temperatures. Cold temperatures ($<$0 °C) are used to argue for the presence of Arc water (i.e., surface AW that is transformed to intermediate water in the Greenland or Iceland Seas). Temperatures between 0 and 3 °C are used to argue for Atl water (i.e., surface AW that has transformed to intermediate water along the Norwegian Continental Slope or Fram Strait) and temperatures greater than 3 °C as an indicator of AW flowing directly over the site within a deepened and stronger NIIC (Våge et al., 2011).

During the process of sea ice growth, the brine rejected from the ice will have differing salinity values, but an unchanged $\delta^{18}O$ due to the invariance of $\delta^{18}O$ with freezing and leads to a flat (close to zero) stable oxygen composition of ocean water (δw) (Craig & Gordon, 1965; Tan & Strain, 1980) while maintaining a low $\delta^{18}O$ and increased salinity (Dokken & Jansen, 1999). Brines are generally formed in shelf areas but can be transported downslope and mixed with different water masses (Dokken et al., 2013; Dokken & Jansen, 1999; Rohling, 2013). Therefore, δ_w is used to support the presence or near-absence of sea ice based on the assumption that the oxygen isotopic signature of the low salinity water where-from sea ice formed and that this makes resultant inmixed waters deviate from the normal salinity/oxygen isotope relation (Craig & Gordon, 1965; Dokken & Jansen, 1999). It is used in this study to argue for the reduced influence of sea ice formation when the δ_w benthics is high ($>$1). We argue for the increased influence of sea ice when δ_w is low ($\approx$0.5).

Although not counted in this study, the high IRD abundances from the PS2644-5 core (Voelker & Haflidason, 2015) are used to indicate periods of the increased presence of icebergs and freshwater. It is also used as an accessory proxy to support the presence of sea ice, as increased iceberg rafting is associated with stadial periods, cold waters with potentially increased sea ice presence (Barker et al., 2015; Dokken et al., 2013).

6. Results

6.1. Benthic Species

The absolute abundance of *C. neoteretis* has its highest values during interstadial periods (up to 66 specimens/g dry bulk sediment; Figure 6). Minimum absolute abundances of *C. neoteretis* (down to zero specimens/sample) are seen subsequent to the highest values during interstadials and at the same time as Mg/Ca ratios of the same species begin to rise. Overall, the absolute abundance of *C. neoteretis* is lower during stadials than during interstadials, but never drops to zero during the stadial. High absolute abundances coincide with heavier values of $\delta^{18}O$ in the same species. The low-resolution counts of *E. excavatum* show an increase in species absolute abundance directly before the largest abundance of *C. neoteretis*. We acknowledge that the counts are only every 5 cm, compared to every 0.5 cm with the *C. neoteretis*, and need higher resolution to be able to say anything concrete concerning the oceanic environment.

6.2. *Cassidulina neoteretis* Stable Isotopes

$\delta^{18}O$ of *C. neoteretis* ($\delta^{18}O_{CN}$) indicates clear variations between two modes with lightest values during the stadials, increasing from 3.9‰ to the heaviest values during the interstadials at 5.6‰ (Figure 6). The transition from heavy to light oxygen isotope composition is gradual, beginning during the interstadial, in contrast to the transitions from stadial to interstadial which are marked by an abrupt increase from light to heavy isotopic values on the onset of the transition. The $\delta^{13}C$ of *C. neoteretis* ($\delta^{13}C_{CN}$) also shows strong phase alignment with the D-O transitions with heavier (up to −0.2‰) values during interstadials and lighter (down to −0.8‰) values during stadials. Transitions on both ends of a D-O cycle in the $\delta^{13}C_{CN}$ signal are abrupt.

6.3. *Cassidulina neoteretis* Mg/Ca

The Mg/Ca results shown in Figure 6 are well aligned with $\delta^{18}O_{CN}$ changes seeing higher values (warmer approximately 0–3 °C) during stadials and lower values (colder approximately −1-1 °C), in general, during interstadials. Both Mg/Ca and $\delta^{18}O_{CN}$ suggests a gradual warming beginning in the middle of the interstadials and have relatively abrupt coolings toward the onset of an interstadial. The Mg/Ca record shows a brief warming just after the onset of an interstadial that is rapid in both onset and offset with similar or higher values than seen during stadials. This is seen clearly in GI 8 and 6, and less clearly in GI 7 and 5, potentially due to lower sampling resolution.

6.4. Ocean Water $\delta^{18}O$

The stable oxygen isotope composition of standard mean ocean water as calculated using the benthic $\delta^{18}O_{CN}$ and Mg/Ca results indicate that the intermediate water is strongly influenced by brine rejection during GS, decreased salinity in the majority of the GI and increased salinity during the interstadial warm episode (Figures 6 and 7). Overall, we see that there is increased salinity or a different originating water mass passing over core site GS15-198-36CC during interstadials than during stadials.

7. Discussion

7.1. Stadials, Mode A

Our Mg/Ca temperature reconstruction (Figure 6) indicates that during GS site GS15-198-36CC was covered by a relatively warm, between 1 and 3 °C, intermediate water mass. Although the Mg/Ca calibrations that are available are not optimal at the extreme cold end, the midrange temperatures are well captured (Barrientos et al., 2018; Kristjánsdóttir et al., 2007). We therefore consider these temperatures calculations to be robust leaving them to fall into the Atl water category according to Våge et al. (2011, 2013) (Figures 6 and 7). Atl water is not optimal for *C. neoteretis*, as it is slightly too warm, and the salinity range associated with Atl. water slightly too fresh (~34.85–34.90 psu), but it has stable conditions and is a cooled Atlantic originating water mass. We see these attributes reflected in the midrange absolute abundance between 5 and 20 specimens/g dry bulk sediment where the specimens are not thriving but are not disappearing either (Figure 6). *Cassidulina neoteretis* is often associated with glacial episodes or periods but are not inclined to excessive IRD as they thrive in fine-grained mud associated with high food availability (Mackensen & Hald, 1988). We do see high influx of IRD within the GS (Figure 6), which we associate with increased iceberg rafting and fresher surface waters but also the presence of sea ice. Sea ice has the potential to have massive phytoplankton blooms and thereby provide the nourishment needed for the benthic foraminifera albeit the rain

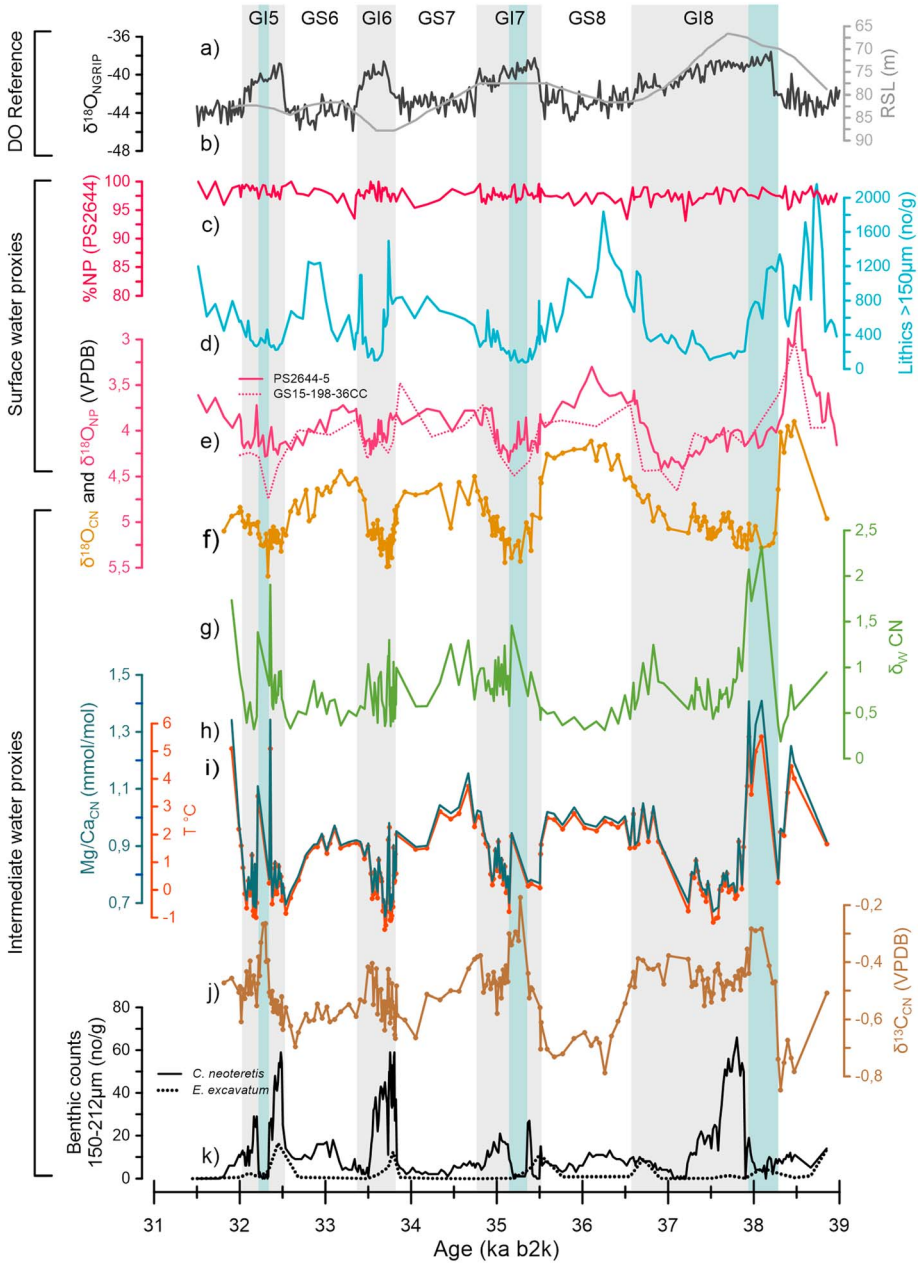

Figure 6. Down core data set from (a) NGRIP, (c–e), PS2644-5 and (e–k) GS15-198-36CC covering the period between 39 to 31.5 ka and D-O events 8–5 on the GICC05 (b2k) age scale. (a) NGRIP $\delta^{18}O$ (proxy for Greenland air temperature and used for age model construction). (b) Relative sea level curve above modern sea level (Waelbroeck et al., 2002). (c) % *N. pachyderma* from core PS2644-5, indicating consistently cold polar water. (d) Lithic grain counts greater than 150 µm (PS2644-5) indicating icebergs and meltwater. (e) $\delta^{18}O$ of *N. pachyderma* (solid line PS2644-5, dotted line GS15-198-36CC) interpreted as a freshwater signal. (f) Benthic $\delta^{18}O$ of *C. neoteretis* aids in reconstructing temperature and salinity. (g) Standard mean ocean water for intermediate water and an indicator for brine contribution. (h) Mg/Ca ratios plotted in mmol/mol for *C. neoteretis*. (i) The temperatures associated with the Mg/Ca values as calculated using equation (2). (j) Benthic $\delta^{13}C$ of *C. neoteretis* used as an indicator for ventilation. (k) Absolute benthic counts plotted per g of dry bulk sediment of *C. neoteretis* (counted every 0.5 cm, solid black line) an indicator for NIIC modified water, and *E. excavatum* (only counted every 5 cm, dotted black line) an indicator for unstable environments. Interstadial periods are noted by grey shading and numbered 8–5, and stadial periods are white. The light turquoise shading indicates Mode C. Lithic grains and *N. pachyderma* data originally published in (Voelker et al., 2000; Voelker & Haflidason, 2015).

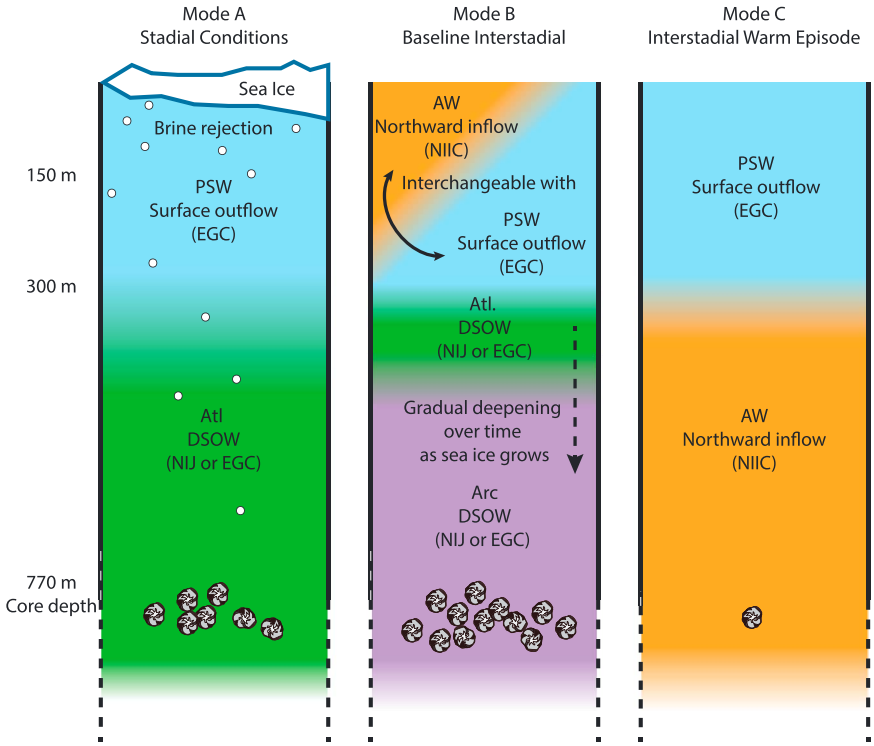

Figure 7. Box schematics showing interpretations for changes in water masses within the water column between modes in the Denmark Strait. Mode A represents the stadial conditions where brine rejection is illustrated by white dots. Mode B the baseline interstadial conditions and Mode C the warm episode that occurs at intermediate depth during an interstadial. The double-sided arrow in Mode B indicates that the surface can switch between summer and winter conditions, as in modern times. The dashed arrow in Mode B indicates the gradual deepening of the Atl toward the end of an interstadial. The *C. neoteretis* at 770 m represents the abundance of species relative to each mode. Note that the core site itself is at 770 m and the suggested depths for surface changes originate from modern observations where the halocline sits at 150 m and the Iceland shelf at approximately 300 m. Acronyms for the water masses are as follows: Polar Surface Water (PSW), Atlantic Originating Water (Atl), Arctic Originating Water (Arc), and Atlantic Water (AW). Currents are bracketed and are as follows: East Greenland Current (EGC), Northern Icelandic Jet (NIJ), and Northern Icelandic Irminger Current (NIIC).

down of extensive IRD (Arrigo et al., 2012; Jennings et al., 2004). Further indications for the presence of sea ice arise from the light $\delta^{18}O_{CN}$, which is in shape and form similar to the NGRIP $\delta^{18}O$ (Figure 6). Dokken et al. (2013) explain this by two different modes of deep water production that are dependent on sea ice conditions. One of which suggests that when sea ice is present, and Greenland is cold, $\delta^{18}O_{CN}$ becomes lighter in the deep Nordic Seas because there is sea ice formation along the Norwegian continental shelf, which creates dense and istopically light brine water that is subsequently transported downward (Craig & Gordon, 1965; Dokken et al., 2013; Dokken & Jansen, 1999). Many studies suggest that little to no open ocean convection took place in the Iceland Sea during GS (Dokken et al., 2013; Ezat et al., 2014; Rasmussen et al., 2016; Rasmussen & Thomsen, 2004).

To further the argument of brines being produced during GS due to the presence of sea ice, we look at the temperature relationship between $\delta^{18}O_{CN}$ and $\delta^{18}O$ of seawater (Figure 6). The oxygen isotopic composition of foraminifera reflects the oxygen isotopic composition of seawater in which the shell calcifies; however it is also dependent on temperature (Marchitto et al., 2014; Ravelo & Hillaire-Marcel, 2007). We notice that the amplitude of the $\delta^{18}O_{CN}$ signal if calculated to be driven by temperature alone is significantly higher than is reasonable in terms of maintaining a stable water column and much smaller than the Mg/Ca-derived temperature amplitude. There should therefore be a residual component of the light $\delta^{18}O_{CN}$ peaks that in the stadial phases that originates from changes in the $\delta^{18}O_w$, presumably caused by influence of water masses with low oxygen isotopic content from brine rejection processes around the basin, as explained in the following: Marchitto et al. (2014) illustrate a temperature dependence of −0.25‰ per °C in cold water. At first

glance, the strong correlation in the stadial mode between the benthic $\delta^{18}O_{CN}$ record and the Mg/Ca-derived benthic temperature reconstructions suggest that $\delta^{18}O_{CN}$ values are largely representative of deepwater temperature changes (Figure 6). However, the changes in $\delta^{18}O_{CN}$ are typically 0.8–1‰ lighter during stadials compared to interstadials, which coincide with an approximate 3–4 °C temperature increase from interstadial to stadial conditions (Figure 6), whereas we see the Mg/Ca changing from approximately −0.5 °C during interstadials to approximately 2 °C during stadials, which is only a 2.5 °C shift. This difference between $\delta^{18}O_{CN}$ and Mg/Ca may be within the potential uncertainty of the methods and Mg/Ca calibration uncertainty; however, as the higher $\delta^{18}O_{CN}$ signal is consistently on the outer end of uncertainties, we infer that brine rejection must also affect the $\delta^{18}O_{CN.}$ At the same time as $\delta^{18}O_{CN}$ is lighter, our $\delta^{13}C_{CN}$ is lighter/lower (Figure 6). As a ventilation indicator, lighter $\delta^{13}C_{CN}$ would suggest reduced surface ventilation (potentially due to sea ice cover and or a strong halocline) with seawater $\delta^{13}C$ influenced by ^{12}C enriched older waters (Dokken et al., 2013).

Supporting evidence in favor of a meltwater cap and sea ice exists from core PS2644-5 (Voelker & Haflidason, 2015), indicating light values of $\delta^{18}O_{NP}$ during stadials in comparison to heavier values during interstadials (Figure 6). The lighter $\delta^{18}O_{NP}$ during stadials indicate either a fresher near surface water, warmer waters at the near surface, or a combination of both to depths of up to 300 m (habitat depth of *N. pachyderma*; Carstens et al., 1997). In agreement with Voelker and Haflidason (2015) we consider that the $\delta^{18}O_{NP}$ is mainly recording a cold fresh surface layer as it is accompanied by a large increase in IRD abundance, and the % *N. pachyderma* is relatively consistent between 95 and 100% indicating consistently cold, polar waters (Voelker & Haflidason, 2015). As icebergs reach waters with temperatures above freezing they begin to melt adding cold, fresh water to the Denmark Strait that, due to its freshness cannot sink to depths and therefore resides at the surface. As the icebergs melt, they release IRD to the Denmark Strait and this is recorded in the sediment from PS2644–5 (Voelker & Haflidason, 2015).

7.2. Transition to Interstadial

Throughout the GS, the warm intermediate water would deepen and expand until reaching a critical point in which connection to the atmosphere takes place, due to a destabilization of the water column causing an overturning and upwelling of warm water to the sea surface. To detect the deepening of the warm intermediate water, we would need a transect of core sites reaching from shallow shelves to the abyssal plain. Hence, our site does not record this deepening. The clearest indicators of overturning and ventilation from our data set come from the synchronized rapid decrease in Mg/Ca values with the increase in $\delta^{18}O_{CN}$, thereby indicating the end of the stadial mode (Figure 6). The most favorable mechanism for causing the rapid changes in ocean water and simultaneously atmospheric conditions over Greenland, as indicated by $\delta^{18}O_{NGRIP}$ is a swift decay of sea ice (Gildor & Tziperman, 2003; Li et al., 2010; Petersen et al., 2013). However, as mechanisms and triggers relating to the abrupt changes between GS and GI is not the focus of this study we do not go into details here.

7.3. Interstadial

Our site records a more complicated GI water column than that of the GS, and we therefore divide it into two modes: Mode B, baseline GI mode, and Mode C, an interstadial warm episode, to explain the shifts in proxies (Figure 7).

7.3.1. Interstadial, Mode B

Mode B, is characterized by benthic Mg/Ca derived temperatures below 0 °C for intermediate water (Figure 6). The Mg/Ca ratios in these time periods are those that are most affected by the alternative calibration (equation (2)) that we use in this study (Figure 4). If we use prepublished calibrations, our Mg/Ca for these periods results in unrealistically cold temperatures (Barrientos et al., 2018; Kristjánsdóttir et al., 2007). This may be because the calibrations are inadequate at the low temperature end or that our site is affected by $\Delta[CO]_3^{2-}$ during cold periods in MIS3 (Elderfield et al., 2006). Our modern core top sample and modern $\Delta[CO]_3^{2-}$ indicate that at present this site is not undersaturated. However, there are no calibrations for calculating $\Delta[CO]_3^{2-}$ for *C. neoteretis* and is needed to further investigate this issue. There are times when the temperatures rise above zero, to ~1 °C; however, this is within likely uncertainty of the Mg/Ca temperature calibration and we therefore feel confident to relate these temperatures to Arc water as denoted by Våge et al. (2011, 2013). To further this argument, *C. neoteretis* peaks (>20 specimens/g dry bulk sediment) during these

periods, especially before the gradual warming begins (Figure 6). *Cassidulina neoteretis* thrives in temperatures around −1 °C, and especially at times with significant food availability, increased sedimentation, and low occurrence of IRD, all of which are indicators of an iceberg and sea ice free (or in any case inconsistent) cover (Jennings et al., 2004; Mackensen & Hald, 1988; Seidenkrantz, 1995).

While Mg/Ca ratio indicates cold temperatures, the $\delta^{18}O_{CN}$, if purely recording temperature, is also indicating a period of cold intermediate waters (Figure 6). When both are used to determine the δ_w, the result is a relatively high value close to 0.5 ‰. This implies that the seawater at depth was not likely affected by brine rejection, such is the Arc water today. Higher $\delta^{13}C_{CN}$ suggests that GI had increased ventilation in comparison to GS (Figure 6). This fits an interpretation where sea ice free conditions and open ocean convection could have occurred in the Iceland Sea, similar to present (Figure 7; Dokken et al., 2013; Ezat et al., 2014; Rasmussen & Thomsen, 2004; Våge et al., 2011; Wary et al., 2017).

Other proxies indicating open water come from the surface records for our site, where we rely on the PS2644-5 record (Voelker et al., 2000; Voelker & Haflidason, 2015). The surface tends to remain fairly consistent between GI showing low IRD depositional periods, and heavy $\delta^{18}O_{NP}$ (Figure 6). We interpret the surface waters to be more saline than during GS as indicated by the heavy $\delta^{18}O_{NP}$ due to less glacial runoff and or iceberg release as indicated by the lower IRD record. Higher salinity could relate to increased AW via the NIIC or a decrease in iceberg discharge and freshwater input. The consistently cold conditions ($>$ 95% *N. pachyderma*) supports the presence of cold surface water, but it is quite probable that the region is made up of PSW in winter and AW in summer as in modern times.

7.3.2. Interstadial Warm Episode, Mode C

Mode C, the interstadial warm episode, is a bit more difficult to explain than Modes A or B, as the proxy-based reconstructions reveals inconsistent timing and intensity of the occurrences. It is clear, however, that a different intermediate water mass and or current is present during these periods. The benthic Mg/Ca values indicate a brief increased warming episode within each GI, defined as, an increase of 2–5 °C from baseline interstadial temperature followed by a return to baseline cold interstadial temperatures that occurs within 50–200 years (Figure 6). For GI8, this occurs almost immediately and is the longest and warmest episode of its type lasting approximately 200 years and reaching up to 6 °C as calculated using equation (2); (Figure 6). For each interstadial warm episode recorded, there is a low absolute abundance of *C. neoteretis* (sometimes disappearing) and the highest recorded $\delta^{13}C_{CN}$ of each interstadial (Figure 6). Low abundance, high temperatures, and increased ventilation indicate a rejuvenation of the NIIC and AW. However, the warm temperature episodes are not recorded or recognized by any changes in the $\delta^{18}O_{CN}$ record. This mode has a large response in estimated SMOW value that hints at large reductions in brine contributions to the water masses with increased salinity that prevents $\delta^{18}O_{CN}$ from becoming lighter when bottom temperatures rise. It is unclear what drives the change in modes, especially since the change does not always occur at the same time within a GI. It is possible that the only real Mode C occurs in GI8, directly after Heinrich events 4 (H4), and the interstadial warm episodes that appear in the other GI's are indicators of some instability in the system and or be a result of lower resolution just at those periods on account of the low abundance of *C. neoteretis*. Increased sampling during these periods, and a full benthic relative abundance reconstruction would aid in the understanding of these episodes.

7.4. Transition to Stadial

All proxies indicate that there is a gradual transition into GS. The Mg/Ca-derived temperature reconstruction indicates a warming trend toward the GS and we interpret this to be gradual deepening of the Atl as sea ice begins to grow towards the end of the GI (Figure 7). This is mirrored by the gradual lightening of $\delta^{18}O_{CN}$, gradual lightening of $\delta^{18}O_{NP}$, gradual increase in IRD and the decrease in *C. neoteretis* absolute abundance.

8. Conclusions

Our results alongside supporting material from site PS2644-5 promote the following interpretations for MIS3 D-O events 8–5. First and foremost, GS appear to be periods of stability whereas GI are relatively unstable, undergoing changes throughout their durations. The Denmark Strait surface and intermediate water masses undergo three distinct modes during D-O events (A, B and C; Figure 7). The stadial mode (Mode A) has a perennial sea ice cover in the western Nordic Seas. The water column is well stratified with a fresh, cold PSW

underlain by warm, brine influenced, Atl Water within the intermediate layer. Low abundance of *C. neoteretis* implies that the warm Atlantic water flowed into the Nordic Seas through the Faeroe-Shetland Channel rather than through the Denmark Strait. Over time the Atl gradually thickened and deepened, flowing out of the Nordic Seas through the Denmark Strait. At some critical time, the water column became unstable and overturned causing sea ice to rapidly disappear; initiating the baseline interstadial mode (Mode B). Mode B comprises an interstadial mode of circulation and water column development similar to modern times with outflowing cool PSW in the EGC at the surface and Arc at depth and inflowing AW via the NIIC on the shelves (and potentially further into the strait during summer). Within each interstadial Mode B there appears to also be a Mode C interval, a period of instability where warming of intermediate water occurs in combination with increased ventilation, increase in salinity, and a drop in *C. neoteretis* abundance. We interpret this as a sudden rejuvenation of warm, saline, AW as NIIC inflow at depth. However, the mechanism for the transition from Mode B to Mode C is unclear, especially as the timing of the mode C between interstadials is different. At some point conditions become ideal to initiate sea ice growth causing gradual reestablishment of a stratified ocean with a strong halocline and the stadial mode is re-established.

Acknowledgments

We thank Rune E. Søraas and Ulysses S. Ninneman for stable isotope analysis and use of FARLAB. We would also like to thank Lisa Griem and Ida Olsen for help in sample preparation and the *R.V. G.O. Sars* crew for successfully retrieving the core in summer 2015. Thanks also go out to the reviewers for constructive comments and improvements to this manuscript. The research leading to these results has received funding from the European Research Council under the European Community's Seventh Framework Programme (FP7/2007-2013) /ERC grant agreement 610055 as part of the Ice2Ice project. All data used in this study are available online through the Pangaea website.

References

Adkins, J. F., McIntyre, K., & Schrag, D. P. (2002). The salinity, temperature, and $\delta^{18}O$ of the Glacial Deep Ocean. *Science*, *298*(5599), 1769–1773. https://doi.org/10.1126/science.1076252

Arrigo, K. R., Perovich, D. K., Pickart, R. S., Brown, Z. W., van Dijken, G. L., Lowry, K. E., et al. (2012). Massive phytoplankton blooms under Arctic sea ice. *Science*, *336*(6087), 1408. https://doi.org/10.1126/science.1215065

Barker, S., Chen, J., Gong, X., Jonkers, L., Knorr, G., & Thornalley, D. (2015). Icebergs not the trigger for North Atlantic cold events. *Nature*, *520*(7547), 333–336. https://doi.org/10.1038/nature14330

Barker, S., Greaves, M., & Elderfield, H. (2003). A study of cleaning procedures used for foraminiferal Mg/Ca paleothermometry. *Geochemistry, Geophysics, Geosystems*, *4*(9), 8407. https://doi.org/10.1029/2003GC000559

Barrientos, N., Lear, C. H., Jakobsson, M., Stranne, C., O'Regan, M., Cronin, T. M., Gukov, A. Y., et al. (2018). Arctic Ocean benthic foraminifera Mg/Ca ratios and global Mg/Ca-temperature calibrations: New constraints at low temperatures. *Geochimica et Cosmochimica Acta*, *236*, 240–259. https://doi.org/10.1016/j.gca.2018.02.036

Boyle, E. A. (1983). Manganese carbonate overgrowths on foraminifera tests. *Geochemica et Cosmochimica Acta*, *47*(10), 1815–1819. https://doi.org/10.1016/0016-7037(83)90029-7

Boyle, E. A., & Keigwin, L. D. (1985/86). Comparison of Atlantic and Pacific paleochemical records for the last 215,000 years: Changes in deep ocean circulation and chemical inventories. *Earth and Planetary Science Letters*, *76*(1-2), 135–150. https://doi.org/10.1016/0012-821X(85)90154-2

Carstens, J., Hebbeln, D., & Wefer, G. (1997). Distribution of planktic foraminifera at the ice margin in the Arctic (Fram Strait). *Marine Micropaleontology*, *29*(3-4), 257–269. https://doi.org/10.1016/S0377-8398(96)00014-X

Craig, H., & Gordon, L. I. (1965). Deuterium and oxygen 18 variations in the ocean and the marine atmosphere. In T. E. (Ed.), *Stable isotopes in oceanographic studies and paleotemperatures* (pp. 9–130). Pisa, Spoleto, Italy: V. Lishi e F.

Dansgaard, W., Johnsen, S. J., Clausen, H. B., Dahl-Jensen, D., Gundestrup, N. S., Hammer, C. U., Hvidberg, C. S., et al. (1993). Evidence for general instability of past climate from a 250 kyr ice-core record. *Nature*, *364*(6434), 218–220. https://doi.org/10.1038/364218a0

Dickson, B., Dye, S., Jónsson, S., Köhl, A., Macrander, A., Marnela, M., Meincke, J., et al. (2008). The overflow flux west of Iceland: Variability, origins and forcing. In R. R. Dickson, J. Meincke, & P. Rhines (Eds.), *Arctic–Subarctic ocean fluxes: Defining the role of the Northern Seas in climate*, (pp. 443–474). Dordrecht: Springer Netherlands. https://doi.org/10.1007/978-1-4020-6774-7_20

Dodd, P. A., Rabe, B., Hansen, E., Falck, E., Mackensen, A., Rohling, E., Stedmon, C., et al. (2012). The freshwater composition of the Fram Strait outflow derived from a decade of tracer measurements. *Journal of Geophysical Research*, *117*, C11005. https://doi.org/10.1029/2012JC008011

Dokken, T., & Jansen, E. (1999). Rapid changes in the mechanism of ocean convection during the last glacial period. *Nature*, *401*(6752), 458–461. https://doi.org/10.1038/46753

Dokken, T. M., Nisancioglu, K. H., Li, C., Battisti, D. S., & Kissel, C. (2013). Dansgaard-Oeschger cycles: Interactions between ocean and sea ice intrinsic to the Nordic seas. *Paleoceanography*, *28*, 491–502. https://doi.org/10.1002/palo.20042

Elderfield, H., Ferretti, P., Greaves, M., Crowhurst, S., McCave, I. N., Hodell, D., & Piotrowski, A. M. (2012). Evolution of ocean temperature and ice volume through the mid-Pleistocene climate transition. *Science*, *337*(6095), 704–709. https://doi.org/10.1126/science.1221294

Elderfield, H., Yu, J., Anand, P., Kiefer, T., & Nyland, B. (2006). Calibrations for benthic foraminiferal Mg/Ca paleothermometry and the carbonate ion hypothesis. *Earth and Planetary Science Letters*, *250*(3–4), 633–649. https://doi.org/10.1016/j.epsl.2006.07.041

Eldevik, T., Nilsen, J. E. Ø., Iovino, D., Anders Olsson, K., Sandø, A. B., & Drange, H. (2009). Observed sources and variability of Nordic seas overflow. *Nature Geoscience*, *2*(6), 406–410. https://doi.org/10.1038/ngeo518

Eynaud, F., Turon, J. L., Matthiessen, J., Kissel, C., Peypouquet, J. P., de Vernal, A., & Henry, M. (2002). Norwegian sea-surface palaeoenvironments of marine oxygen-isotope stage 3: The paradoxical response of dinoflagellate cysts. *Journal of Quaternary Science*, *17*(4), 349–359. https://doi.org/10.1002/jqs.676

Ezat, M. M., Rasmussen, T. L., & Groeneveld, J. (2014). Persistent intermediate water warming during cold stadials in the southeastern Nordic seas during the past 65 k.y. *Geology*, *42*(8), 663–666. https://doi.org/10.1130/G35579.1

Ezat, M. M., Rasmussen, T. L., Honisch, B., Groeneveld, J., & deMenocal, P. (2017). Episodic release of CO2 from the high-latitude North Atlantic Ocean during the last 135 kyr. *Nature Communications*, *8*, 14498. https://doi.org/10.1038/ncomms14498

Gildor, H., & Tziperman, E. (2003). Sea-ice switches and abrupt climate change. *Philosophical Transactions of the Royal Society of London. Series A*, *36*(1810), 1935–1944.

Greaves, M., Caillon, N., Rebaubier, H., Bartoli, G., Bohaty, S., Cacho, I., Clarke, L., et al. (2008). Interlaboratory comparison study of calibration standards for foraminiferal Mg/Ca thermometry. *Geochemistry, Geophysics, Geosystems*, *9*, Q08010. https://doi.org/10.1029/2008GC001974

Groeneveld, J., & Filipsson, H. L. (2013). Mg/Ca and Mn/Ca ratios in benthic foraminifera: The potential to reconstruct past variations in temperature and hypoxia in shelf regions. *Biogeosciences*, *10*(7), 5125–5138. https://doi.org/10.5194/bg-10-5125-2013

Hald, M., Steinsund, P., Dokken, T., Korsun, S., Polyak, L., & Aspeli, R. (1994). Recent and Late Quaternary distribution of Elphidium excavatum F. clavatum in Arctic Seas. *Cushman Foundation Special Publications*, *32*, 141–153.

Hasenfratz, A. P., Martínez-García, A., Jaccard, S. L., Vance, D., Wälle, M., Greaves, M., & Haug, G. H. (2017). Determination of the Mg/Mn ratio in foraminiferal coatings: An approach to correct Mg/Ca temperatures for Mn-rich contaminant phases. *Earth and Planetary Science Letters*, *457*, 335–347. https://doi.org/10.1016/j.epsl.2016.10.004

Jansen, E., Sjøholm, J., Bleil, U., & Erichsen, J. A. (1990). Neogene and Pleistocene glaciations in the northern hemisphere and Late Miocene-Pliocene global ice volume fluctuations: Evidence from the Norwegian Sea. In U. Bleil & J. Thiede (Eds.), *Geological history of the Polar Oceans: Arctic Versus Antarctic* (pp. 677–705). Dordrecht: Springer Netherlands. https://doi.org/10.1007/978-94-009-2029-3_35

Jeansson, E., Jutterström, S., Rudels, B., Anderson, L. G., Anders Olsson, K., Jones, E. P., Smethie, W. M., et al. (2008). Sources to the East Greenland Current and its contribution to the Denmark Strait Overflow. *Progress in Oceanography*, *78*(1), 12–28. https://doi.org/10.1016/j.pocean.2007.08.031

Jennings, A. E., & Helgadottir, G. (1994). Foraminiferal assemblages from the fjords and shelf of eastern Greenland. *The Journal of Foraminiferal Research*, *24*(2), 123–144. https://doi.org/10.2113/gsjfr.24.2.123

Jennings, A. E., Weiner, N., Helgadottir, G., & Andrews, J. T. (2004). Modern foraminiferal faunas of the Southwestern to Northern Iceland shelf: Oceanographic and environmental controls. *Journal of Foraminiferal Research*, *34*(3), 180–207. https://doi.org/10.2113/34.3.180

Jonsson, S., & Valdimarsson, H. (2004). A new path for the Denmark Strait overflow water from the Iceland Sea to Denmark Strait. *Geophysical Research Letters*, *31*, L03305. https://doi.org/10.1029/2003GL019214

Jonsson, S., & Valdimarsson, H. (2012). Hydrography and circulation over the southern part of the Kolbeinsey ridge. *ICES Journal of Marine Science*, *69*(7), 1255–1262. https://doi.org/10.1093/icesjms/fss101

Kissel, C., Laj, C., Labeyrie, L., Dokken, T., Voelker, A., & Blamart, D. (1999). Rapid climatic variations during marine isotopic stage 3: Magnetic analysis of sediments from Nordic seas and North Atlantic. *Earth and Planetary Science Letters*, *171*(3), 489–502. https://doi.org/10.1016/S0012-821X(99)00162-4

Köhl, A., Käse, R. H., Stammer, D., & Serra, N. (2007). Causes of changes in the Denmark Strait overflow. *Journal of Physical Oceanography*, *37*(6), 1678–1696. https://doi.org/10.1175/JPO3080.1

Kristjánsdóttir, G. B., Lea, D. W., Jennings, A. E., Pak, D. K., & Belanger, C. (2007). New spatial Mg/Ca-temperature calibrations for three Arctic, benthic foraminifera and reconstruction of North Iceland shelf temperature for the past 4000 years. *Geochemistry, Geophysics, Geosystems*, *8*, Q03P21. https://doi.org/10.1029/2006GC001425

Laj, C. (2003). *Paleomagnetic of sediment core PS2644–5*. PANGAEA. Retrieved from https://doi.org/10.1594/PANGAEA.118604

Li, C., Battisti, D. S., & Bitz, C. M. (2010). Can North Atlantic Sea ice anomalies account for Dansgaard–Oeschger climate signals? *Journal of Climate*, *23*(20), 5457–5475. https://doi.org/10.1175/2010JCLI3409.1

Logemann, K., & Harms, I. (2006). High resolution modelling of the North Icelandic Irminger Current (NIIC). *Ocean Science*, *2*(2), 291–304. https://doi.org/10.5194/os-2-291-2006

Lorenz, A. (2005). Variability of benthic foraminifera north and south of the Denmark Strait, Doctoral Thesis thesis, 139 pp, Christian-Albrechts Univ. of Kiel, Kiel.

Lubinski, D. J., Polak, L., & Forman, S. L. (2001). Freshwater and Atlantic water inflows to the deep northern Barents and Kara seas since ca 13 14C ka: Foraminifera and stable isotopes. *Quaternary Science Reviews*, *20*(18), 1851–1879. https://doi.org/10.1016/S0277-3791(01)00016-6

Lueker, T. J., Dickson, A. G., & Keeling, C. D. (2000). Ocean pCO2 calculated from dissolved inorganic carbon, alkalinity, and equations for K1 and K2: Validation based on laboratory measurements of CO2 in gas and seawater at equilibrium. *Marine Chemistry*, *70*(1-3), 105–119. https://doi.org/10.1016/S0304-4203(00)00022-0

Mackensen, A., & Hald, M. (1988). *Cassidulina teretis* Tappan and *Laevigata* D'Orbigny: Their modern and Late Quaternary distribution in northern seas. *Journal of Foraminiferal Research*, *18*(1), 16–24. https://doi.org/10.2113/gsjfr.18.1.16

Marchitto, T. M., Curry, W. B., Lynch-Stieglitz, J., Bryan, S. P., Cobb, K. M., & Lund, D. C. (2014). Improved oxygen isotope temperature calibrations for cosmopolitan benthic foraminifera. *Geochimica et Cosmochimica Acta*, *130*, 1–11. https://doi.org/10.1016/j.gca.2013.12.034

Mauritzen, C., & Häkkinen, S. (1997). Influence of sea ice on the thermohaline circulation in the Arctic-North Atlantic Ocean. *Geophysical Research Letters*, *24*(24), 3257–3260. https://doi.org/10.1029/97GL03192

Millero, F. J., Chen, C.-T., Bradshaw, A., & Schleicher, K. (1980). A new high pressure equation of state for seawater. *Deep Sea Research Part A. Oceanographic Research Papers*, *27*(3-4), 255–264. https://doi.org/10.1016/0198-0149(80)90016-3

Nilsen, J. E. Ø., Gao, Y., Drange, H., Furevik, T., & Bentsen, M. (2003). Simulated North Atlantic-Nordic Seas water mass exchanges in an isopycnic coordinate OGCM. *Geophysical Research Letters*, *30*(10), 1536. https://doi.org/10.1029/2002GL016597

Olsen, A., Key, R. M., van Heuven, S., Lauvset, S. K., Velo, A., Lin, X., Schirnick, C., et al. (2016). The Global Ocean Data Analysis Project version 2 (GLODAPv2)—An internally consistent data product for the world ocean. *Earth System Science Data*, *8*(2), 297–323. https://doi.org/10.5194/essd-8-297-2016

Paillard, D., Labeyrie, L., & Yiou, P. (1996). Macintosh program performs time-series analysis. *EOS Transactions American Geoophysical Union*, *77*(39), 379. https://doi.org/10.1029/96EO00259

Petersen, S. V., Schrag, D. P., & Clark, P. U. (2013). A new mechanism for Dansgaard-Oeschger cycles. *Paleoceanography*, *28*, 24–30. https://doi.org/10.1029/2012PA002364

Rahmstorf, S. (2002). Ocean circulation and climate during the past 120,000 years. *Nature*, *419*(6903), 207–214. https://doi.org/10.1038/nature01090

Rasmussen, S. O., Bigler, M., Blockley, S. P., Blunier, T., Buchardt, S. L., Clausen, H. B., Cvijanovic, I., et al. (2014). A stratigraphic framework for abrupt climatic changes during the Last Glacial period based on three synchronized Greenland ice-core records: Refining and extending the INTIMATE event stratigraphy. *Quaternary Science Reviews*, *106*, 14–28. https://doi.org/10.1016/j.quascirev.2014.09.007

Rasmussen, T. L., & Thomsen, E. (2004). The role of the North Atlantic Drift in the millennial timescale glacial climate fluctuations. *Palaeogeography, Palaeoclimatology, Palaeoecology*, *210*(1), 101–116. https://doi.org/10.1016/j.palaeo.2004.04.005

Rasmussen, T. L., Thomsen, E., & Moros, M. (2016). North Atlantic warming during Dansgaard-Oeschger events synchronous with Antarctic warming and out-of-phase with Greenland climate. *Scientific Reports*, *6*(1), 20,535. https://doi.org/10.1038/srep20535

Ravelo, A. C., & Hillaire-Marcel, C. (2007). Chapter Eighteen The use of oxygen and carbon isotopes of foraminifera in paleoceanography. *Developments in Marine Geology*, *1*, 735–764.

Risebrobakken, B., Jansen, E., Andersson, C., Mjelde, E., & Hevrøy, K. (2003). A high-resolution study of Holocene paleoclimatic and paleoceanographic changes in the Nordic Seas. *Paleoceanography*, *18*(1), 1017. https://doi.org/10.1029/2002PA000764

Rohling, E. J. (2013). Oxygen isotope composition of seawater. In S. A. Elias (Ed.), *Encyclopedia of Quaternary Science* (Vol. 2, pp. 915–922). Amsterdam: Elsevier.

Rosenthal, Y., Field, M. P., & Sherrell, R. M. (1999). Precise determination of element/calcium ratios in calcareous samples using sector field inductively coupled plasma mass spectrometry. *Analytical Chemistry*, *71*(15), 3248–3253. https://doi.org/10.1021/ac981410x

Rudels, B. (2002). The East Greenland Current and its contribution to the Denmark Strait overflow. *ICES Journal of Marine Science*, *59*(6), 1133–1154. https://doi.org/10.1006/jmsc.2002.1284

Rudels, B., Björk, G., Nilsson, J., Winsor, P., Lake, I., & Nohr, C. (2005). The interaction between waters from the Arctic Ocean and the Nordic Seas north of Fram Strait and along the East Greenland Current: Results from the Arctic Ocean-02 Oden expedition. *Journal of Marine Systems*, *55*(1–2), 1–30. https://doi.org/10.1016/j.jmarsys.2004.06.008

Rudels, B., Muench, R. D., Gunn, J., Schauer, U., & Friedrich, H. J. (2000). Evolution of the Arctic Ocean boundary current north of the Siberian shelves. *Journal of Marine Systems*, *25*(1), 77–99. https://doi.org/10.1016/S0924-7963(00)00009-9

Rytter, F., Knudsen, K. L., Seidenkrantz, M.-S., & Eiríksson, J. (2002). Modern distribution of benthic foraminifera on the North Icelandic Shelf and Slope. *The Journal of Foraminiferal Research*, *32*(3), 217–244. https://doi.org/10.2113/32.3.217

Schlitzer, R. (2014). Ocean data view.

Schrag, D. P., Hampt, G., & Murray, D. W. (1996). Pore fluid constraints on the temperature and oxygen isotopic composition of the Glacial Ocean. *Science*, *272*(5270), 1930–1932. https://doi.org/10.1126/science.272.5270.1930

Seidenkrantz, M. S. (1995). Cassidulina teretis Tappan and Cassidulina neoteretis new species (foraminifera): Stratigraphic markers for deep sea and outer shelf areas. *Journal of Micropalaeontology*, *14*(2), 145–157. https://doi.org/10.1144/jm.14.2.145

Shackleton, N. J. (1974). Attainment of isotopic equilibrium between ocean water and the benthonic foraminifera genus Uvigerina: Isotopic changes in the ocean during the last glacial. *Colloques Internationaux du Centre National de la Recherche Scientifique*, *219*, 203–209.

Skinner, L. C., Shackleton, N. J., & Elderfield, H. (2003). Millennial-scale variability of deep-water temperature and δ18Odw indicating deep-water source variations in the Northeast Atlantic, 0–34 cal. ka BP. *Geochemistry, Geophysics, Geosystems*, *4*(12), 1098. https://doi.org/10.1029/2003GC000585

Skirbekk, K., Hald, M., Marchitto, T. M., Junttila, J., Kristensen, D. K., & Sørensen, S. A. (2016). Benthic foraminiferal growth seasons implied from mg/ca-temperature correlations for three Arctic species. *Geochemistry, Geophysics, Geosystems*, *17*, 4684–4704. https://doi.org/10.1002/2016GC006505

Solignac, S., Giraudeau, J., & de Vernal, A. (2006). Holocene sea surface conditions in the western North Atlantic: Spatial and temporal heterogeneities. *Paleoceanography*, *21*, PA2004. https://doi.org/10.1029/2005PA001175

Svensson, A., Andersen, K. K., Bigler, M., Clausen, H. B., Dahl-Jensen, D., Davies, S. M., Johnsen, S. J., et al. (2008). A 60 000 year Greenland stratigraphic ice core chronology. *Climate of the Past*, *4*(1), 47–57. https://doi.org/10.5194/cp-4-47-2008

Swift, J. H., & Aagaard, K. (1981). Seasonal transitions and water mass formation in the Iceland and Greenland seas. *Deep Sea Research Part A. Oceanographic Research Papers*, *28*(10), 1107–1129. https://doi.org/10.1016/0198-0149(81)90050-9

Tan, F. C., & Strain, P. M. (1980). The distribution of sea ice meltwater in the eastern Canadian Arctic. *Journal of Geophysical Research*, *85*(C4), 1925. https://doi.org/10.1029/JC085iC04p01925

Våge, K., Pickart, R. S., Spall, M. A., Moore, G. W. K., Valdimarsson, H., Torres, D. J., Erofeeva, S. Y., et al. (2013). Revised circulation scheme north of the Denmark Strait. *Deep Sea Research Part I: Oceanographic Research Papers*, *79*, 20–39. https://doi.org/10.1016/j.dsr.2013.05.007

Våge, K., Pickart, R. S., Spall, M. A., Valdimarsson, H., Jónsson, S., Torres, D. J., Østerhus, S., et al. (2011). Significant role of the North Icelandic Jet in the formation of Denmark Strait overflow water. *Nature Geoscience*, *4*(10), 723–727. https://doi.org/10.1038/ngeo1234

van Kreveld, S., Sarnthein, M., Erlenkeuser, H., Grootes, P., Jung, S., Nadeau, M. J., Pflaumann, U., et al. (2000). Potential links between surging ice sheets, circulation changes, and the Dansgaard-Oeschger cycles in the Irminger Sea, 60-18 Kyr. *Paleoceanography*, *15*(4), 425–442. https://doi.org/10.1029/1999PA000464

Voelker, A. (2002). Global distribution of centennial-scale records for Marine Isotope Stag (MIS) 3: A database. *Quaternary Science Reviews*, *21*(10), 1185–1212. https://doi.org/10.1016/S0277-3791(01)00139-1

Voelker, A., Grootes, P., Nadeau, M. J., & Sarnthein, M. (2000). Radiocarbon levels in the Iceland Sea from 25-53 kyr and their link to the Earth's magnetic field intensity. *Radiocarbon*, *42*(03), 437–452. https://doi.org/10.1017/S0033822200030368

Voelker, A. H. L., & Haflidason, H. (2015). Refining the Icelandic tephrachronology of the last glacial period – The deep-sea core PS2644 record from the southern Greenland Sea. *Global and Planetary Change*, *131*, 35–62. https://doi.org/10.1016/j.gloplacha.2015.05.001

Voelker, A. H. L., Sarnthein, M., Grootes, P. M., Erlenkeuser, H., Laj, C., Mazaud, A., Nadeau, M.-J., et al. (1998). Correlation of marine ^{14}C ages from the Nordic seas with the GISP2 isotope record: Implications for 14C calibration beyond 25 ka BP. *Radiocarbon*, *40*(01), 517–534.

Waelbroeck, C., Labeyrie, L., Michel, E., Duplessy, J. C., McManus, J. F., Lambeck, K., Balbon, E., et al. (2002). Sea-level and deep water temperature changes derived from benthic foraminifera isotopic records. *Quaternary Science Reviews*, *21*(1–3), 295–305. https://doi.org/10.1016/S0277-3791(01)00101-9

Wary, M., Eynaud, F., Marjolaine, S., Zaragosi, S., Rossignol, L., Malaizé, B., Palis, E., et al. (2015). Stratification of surface waters during the last glacial millennial climatic events: A key factor in subsurface and deep water mass dynamics. *Climate of the Past Discussions*, *11*(3), 2077–2119. https://doi.org/10.5194/cpd-11-2077-2015

Wary, M., Eynaud, F., Rossignol, L., Zaragosi, S., Sabine, M., Castera, M.-H., & Billy, I. (2017). The southern Norwegian Sea during the last 45 ka: Hydrographical reorganizations under changing ice-sheet dynamics. *Journal of Quaternary Science*, *32*(7), 908–922. https://doi.org/10.1002/jqs.2965